


Spaceborne Altimeter Calibration System With Calibration Satellites

Chenghao Lu, *Graduate Student Member, IEEE*, Taoli Yang , *Senior Member, IEEE*,
Boxiang Zhang, *Member, IEEE*, and Hanwen Yu , *Senior Member, IEEE*

Abstract—Spaceborne altimeters are indispensable tools in the aerospace and Earth science fields, and ensuring their accuracy is paramount. However, their accuracy is affected by various factors, including systematic and atmospheric attenuations. This study explores an altimeter calibration system based on a calibration satellite equipped with a transponder. When the altimeter passes directly over the calibration satellite, the transponder facilitates signal interaction with the altimeter, serving as a stable reference point to effectively calibrate the altimeter’s systematic errors. In addition, a network optimization scheme based on the nondominated sorting generic algorithm-II is proposed to enhance the calibration accuracy and networking efficiency of the calibration system. Error analysis and network simulation results prove the feasibility of the proposed system.

Index Terms—Backscatter coefficient, calibration satellites, network optimization, and spaceborne altimeters.

I. INTRODUCTION

MICROWAVE remote sensing technology emerged in the 1950s, offering the advantages of strong monitoring ability, wide coverage area, low cost, and all-day, all-weather measurements [1]. The spaceborne radar altimeter is one of the main components of microwave remote sensing, it can obtain information on the effective wave height of the sea surface and measure the backscattering coefficient to determine the wind speed over the ocean. Sea dynamic data acquired by radar altimeters have become an essential foundation for physical oceanography, geodesy, and other disciplines [2], [3]. So far, different series of altimeter have been launched worldwide, including the early SEASAT [4], and GEOsat [5] to the current Jason-3 [6], Sentinel-3 [7], and HY series altimeter [8], [9], [10], [11]. In addition, the data observation accuracy has increased from the meter to the centimeter level [3].

Calibration of the satellite sensors is an important prerequisite for quantitative remote sensing to ensure accurate judgment.

Received 9 August 2024; revised 11 September 2024; accepted 17 September 2024. Date of publication 30 September 2024; date of current version 21 October 2024. This work was supported in part by the National Natural Science Foundation of China under Grant 42271456, and in part by the Natural Science Foundation of Sichuan Province under Grant 2022NSFSC0954. (*Corresponding author: Taoli Yang.*)

Chenghao Lu, Taoli Yang, and Hanwen Yu are with the School of Resources and Environment, University of Electronic Science and Technology of China, Chengdu 611731, China (e-mail: lch0008123@163.com; yangtl@uestc.edu.cn; yuhanwenxd@gmail.com).

Boxiang Zhang is with the Millimeter Wave Imaging Technology Laboratory, Shanghai Institute of Satellite Engineering, Shanghai 201109, China (e-mail: zbxshanghai@163.com).

Digital Object Identifier 10.1109/JSTARS.2024.3470775

Calibrating the altimeter’s scattering coefficient in orbit improves the precision of wind speed measurements and ensures stable and accurate data.

Passive calibration [12], cross-calibration [13], [14], [15], uniform natural scene calibration [16], and active calibration methods based on scaler [17], [18] have been proposed to calibrate the backscatter coefficient of altimeter. Passive calibration technology is mainly used for altimeters operating in the “noise-listening” mode (i.e., in the absence of a transmitted pulse). Power [19] received by an altimeter using the sea echo equation in “noise-listening” mode is used to facilitate radiometry to measure different targets (such as water, ice, and forest). The calibration process is completed by considering the receiver gain and its fluctuations. The final determination of the calibrated backscatter coefficient depends on the accuracy of the noise level estimation observed by the altimeter in passive mode.

The cross-calibration method is used to compare the measurement results of two or more altimeters, one of which is considered to have been accurately calibrated by a certain method (considered as a reference), and the others can be compared with it to obtain the measurement deviation of the remaining satellite altimeters [20], which is the relative calibration method. Using distributed target imaging from natural calibration sites on the Earth’s surface, Shimada et al. [16] obtained antenna patterns of satellite instruments based on the Amazon rainforest, aiming to improve estimation accuracy. However, this method has technical limitations and cannot meet future application requirements for all-weather altimeters.

The active calibration method based on scaler involves setting up a scaler in artificial calibration sites, and its radar scattering cross-section is achieved through self-calibration. During calibration, the altimeter operates in the Preset Loop Output mode, and the calibration error is corrected by analyzing the measured echo and absolute powers. The scalars can be divided into passive and active scalars based on their implementation. A passive scaler uses an angle reflector or metal ball, whereas an active scaler (transponder [21]) is a radar auxiliary equipment to receive the signal and return the altimeter after amplification.

A uniform natural scene is suitable for the X band and below. Moreover, the penetration of the high-frequency band is weak, and the radar echoes in rainforests are concentrated in the canopy area. The effectiveness of this scenario for high-frequency and high-resolution calibration has not been demonstrated. However, uniform calibration fields have been destroyed by humans. For example, between August 2020 and July 2021, the Amazon

rainforest shrank by 10 476 km², roughly the size of nine Rio de Janeiro cities. Moreover, locating an artificial calibration field and establishing large-scale centralization is challenging, which restricts the measurement requirements for altimeter multifrequency calibration. Moreover, directly separating the coupled atmospheric attenuation and systematic errors is challenging, which restricts the calibration accuracy.

To solve this problem, we propose a novel spaceborne calibration system that uses calibration satellites. This method moves the transponder from the ground to the calibration satellite using the active calibration method based on scalar. The atmospheric and systematic errors are indirectly separated using the signal power receiving model of the dual-link. Simultaneously, a satellite network based on the nondominated sorting genetic algorithm-II (NSGA-II) of the improved genetic algorithm is proposed [22] to realize multifrequency calibration by considering the service frequency and number of serviceable satellites.

The rest of this article is organized as follows. The radar equation and traditional active calibration method based on a transponder are reviewed in Section II. Section III proposes a novel calibration system based on calibration satellites and the satellite network. The results of the network simulation and error analysis are presented in Section IV. Finally, Section V concludes this article.

II. REVIEW OF TRADITIONAL CALIBRATION METHOD

A. Radar Equation

The directional nature of radar [23] ensures that the energy in one direction is more effective than that in others. Gain refers to the ratio of the power density radiated over a long distance in a specific direction to the power density of an isotropic antenna radiating the same power at the same distance. In 1975, Wheeler proposed the antenna theory, which explained the connection between antenna gain and effective area.

$$G = \frac{4\pi A_e}{\lambda^2} \quad (1)$$

where λ is the wavelength and A_e is the effective area of the antenna.

Then, the power density at distance R between the radar and target can be obtained as follows:

$$S_t = \frac{P_t G}{4\pi R^2} \quad (2)$$

where S_t is the power density and P_t is the power of the transmitted echo.

During transmission and reception, part of the energy is intercepted by the target and then radiated in various directions. The energy radiated in different directions varies. The power density reradiated toward the radar determines the final signal power acquired by the radar. S_a is considered an imaginary area that captures all the energy that falls vertically onto it and then isotropically radiates it to facilitate the characterization of the scattering properties of the target. The power of the received

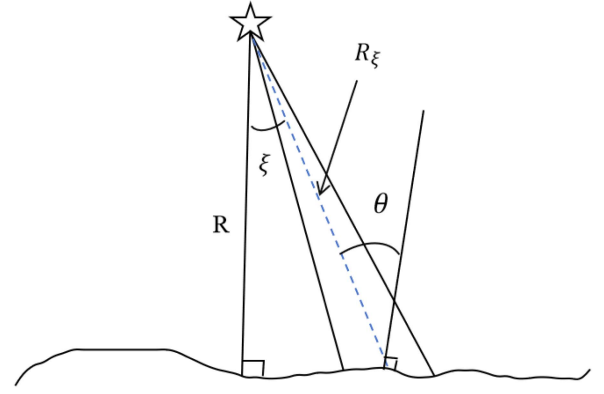


Fig. 1. Altimeter to sea surface beam diagram.

echo can be expressed as follows:

$$P_r = \frac{P_t G^2 \lambda^2 S_a}{(4\pi)^3 R^4} \quad (3)$$

However, because of atmospheric attenuation, the electromagnetic waves emitted by the altimeter are attenuated during propagation to the surface, and the transmitted echo and received backscatter powers can vary. The sea surface was taken as an example to analyze the altimeter signal reception, as shown in Fig. 1. R is the distance from the altimeter satellite to the sea surface [24], ξ is the pointing angle of the altimeter antenna, and A_f is the antenna irradiation area.

In 1993, Wheeler [25] proved that, for altimeters, when the angle of incidence is less than 1°, and the geoid undulation is less than 10⁻⁴, R and R_ξ can be considered equal. The expression for the received power can then be obtained using integration.

$$dP_r = t^2 \frac{G^2 \lambda^2 P_t}{(4\pi)^3 R^4} \sigma_0 \quad (4)$$

where t is the atmospheric attenuation factor and σ_0 is a parameter that represents the radar cross-sectional factor of different target areas dA . $\sigma_0 = \sigma dA$ is used to characterize the average scattering characteristics in the antenna footprint.

By replacing t^2 with the reciprocal of L_p and substituting the area $A = \pi R c \tau_p$ into (4), the received power from the surface target can be obtained as follows:

$$P_r = \frac{G^2 \lambda^2 P_t}{(4\pi)^3 R^4 L_p} \pi R c \tau_p \sigma \quad (5)$$

where τ_p is the pulsewidth, c is the speed of light, and L_p is the propagation loss.

B. Traditional Active Altimeter Calibration Method

Currently, to improve calibration accuracy, ground-based transponders are deployed to relay the echo received by the altimeter. A transponder is an auxiliary satellite radar device that receives an altimeter signal and transmits the amplified signal to the signal source after retransportation. Therefore, it can be seen as a precisely defined reflection target. Transponder-assisted calibration for altimeters was used for TOPEX/Poseidon altimeter calibration as early as 1991 and is known as the active

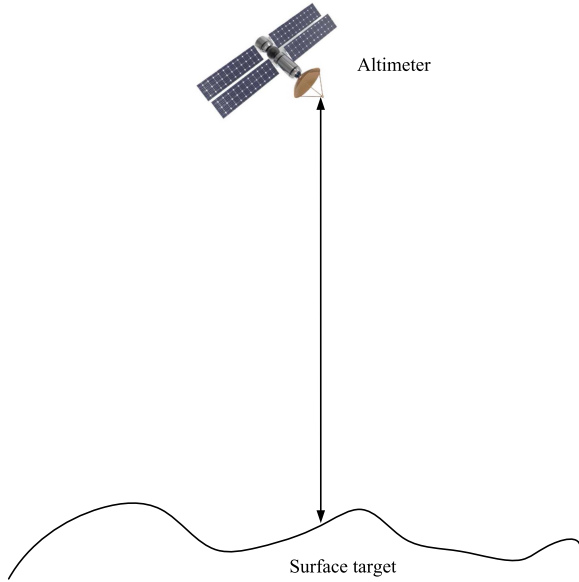


Fig. 2. Traditional calibration diagram.

transponder for altimeter calibration [26]. China's Marine Power Environment Satellite Haiyang-2A (HY-2A), is also equipped with a reconstructed transponder, which is believed to have high precision and can be used directly [27], [28], [29], [30].

The traditional calibration methods are basically single links. The signal is transmitted from the altimeter and reflected by the ground target. The altimeter accepts the echo and carries out the required coefficient correction, as shown in Fig. 2.

In this study, the transponder can be used to obtain more accurate parameters in (5) and provide more significant scattering characteristics than ground objects. The calculated backscattering coefficient error is eliminated according to the existing atmospheric model to complete the calibration of the backscattering coefficient of the altimeter.

$$\sigma = \frac{64\pi^2 R^3 L_p P_r}{G^2 \lambda^2 P_t c \tau_p} \quad (6)$$

III. NOVEL ALTIMETER CALIBRATION SYSTEM

A. Altimeter Calibration Method Using Calibration Satellite

Under the premise that the data reflected by the transponder are highly precise, the next step is to constantly revise the atmospheric models. However, the remaining errors were considered to be coupled with atmospheric and system parameter errors; therefore, correcting the atmospheric error alone is not sufficient to effectively correct the overall error, which brings challenges to the traditional calibration scheme.

The coupling error will occur owing to the atmospheric interference between the scatterer and altimeter. Therefore, we propose launching a calibration satellite equipped with a transponder into space, as shown in Fig. 3.

A link is added based on the original single-link system. Hence, the new system can be called a dual-link system, namely, "altimeter-calibration satellite" and "altimeter-surface target." The "altimeter-surface target" obeys the principle of the traditional calibration method, expressed using (6). In addition,

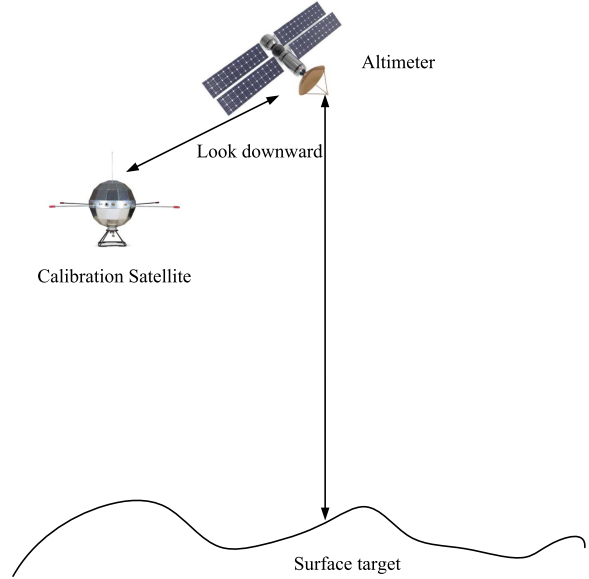


Fig. 3. Diagram of dual-link calibration geometry.

the term "calibration satellite" includes all the functions of a transponder unless otherwise stated.

By moving the transponder from ground to space, the altimeter of the dual-link system processes two types of signals: one from the surface target and another from the calibration satellite. Once the transponder moves, the signal from the calibration satellites does not need to penetrate the atmosphere; thus, there is no attenuation owing to atmospheric influences. The equations for the two links can be obtained by changing the corresponding parameters based on the radar equation. If any terms are identical, we could replace those terms in "altimeter-surface target" with the same in "altimeter-calibration satellite." The specific flow chart is shown in Fig. 4. The calibration process is divided considering the following three aspects.

1) *Interaction of the Altimeter With the Calibration Satellite*: The orbit of the calibration satellite is slightly lower than the orbital height of the downward-looking altimeter. Thus, the altimeter can receive the echo signal of the calibration satellite when it passes directly under the altimeter. Considering the influence of the antenna pattern combined with (5), the received signal can be expressed as follows:

$$P_r = \frac{P_t G^2 \lambda^2}{(4\pi)^3 R_s^4} \sigma_{\text{trans}} f_{\text{alt}}^2(\theta_A, \phi) f_{\text{trans}}^2(\theta_A, \phi) \quad (7)$$

where R_s is the distance between the altimeter and calibration satellite, σ is the backscatter coefficient of the transponder mounted on the calibration satellite, $f_{\text{alt}}(\theta_A, \phi)$ and $f_{\text{trans}}(\theta_A, \phi)$ are the antenna patterns of the altimeter and calibration satellite, respectively, and θ_A and ϕ are the azimuth and inclination, respectively.

The output from the altimeter is digital, and the results achieved should have multiple receiver system gains G_{sys} .

$$DN_{At} = \frac{P_t G^2 \lambda^2}{(4\pi)^3 R_s^4} G_{\text{sys}} \sigma_{\text{trans}} f_{\text{alt}}^2(\theta_A, \phi) f_{\text{trans}}^2(\theta_A, \phi). \quad (8)$$

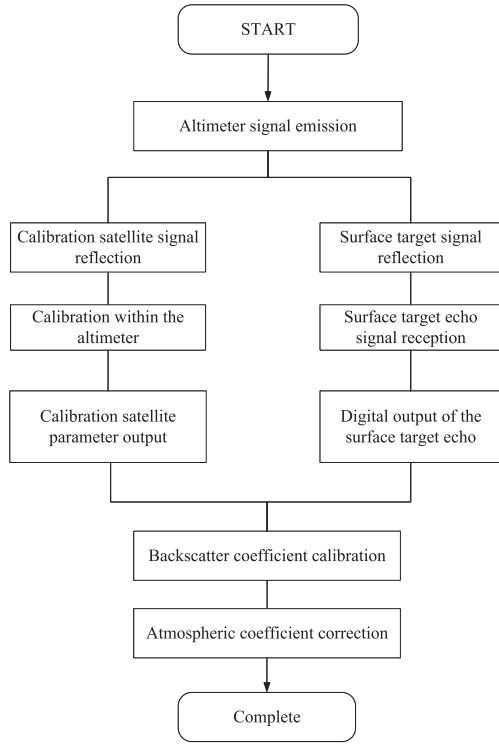


Fig. 4. Flow chart of the novel altimeter calibration system.

Considering that the measurements acquired by the calibration satellite are of high accuracy, the terms in (8) can be used for correcting the link “altimeter-surface target.”

2) *Interaction of the Altimeter With the Surface Target:* This link can directly utilize the relevant framework of the traditional altimeter calibration method, as described in Section II. The digital output can be achieved by replacing the corresponding parameters of (5), as follows:

$$DN_A = P_r G_{sys} = \frac{G^2 \lambda^2 P_t}{(4\pi)^3 R^4 L_p} G_{sys} \pi R c \tau_p \sigma \quad (9)$$

where λ is the wavelength, σ is the backscattering coefficient, R is the distance between the altimeter and target, and τ_p is the pulsewidth.

For an explicitly scaled object, (9) can be written as an expression of the backscattering coefficient σ as follows:

$$\sigma = \frac{64\pi^2 R^3 L_p DN_A}{G^2 \lambda^2 P_t G_{sys} c \tau_p} \quad (10)$$

3) *Dual Link Joint Calibration:* Some terms in (8) and (9) are the same. The data from the calibration satellite discard a considerable part of the atmospheric interference compared to the surface target echo, providing an accurate correction of the system parameters. By combining the two equations, a new expression for the backscatter coefficient can be obtained.

$$\sigma = \frac{DN_A R^3}{DN_{At} R_s^4} \frac{1}{c \tau_p \pi L_{pt}} f_{alt}^2(\theta_A, \phi) f_{trans}^2(\theta_A, \phi) \sigma_{trans} \quad (11)$$

This is to say, the terms from the link “altimeter-surface target” has systematic errors and errors due to atmospheric attenuation. However, similar terms in the link “altimeter-calibration satellite” are much more precise, as it eliminates atmospheric interference. Thus, only systematic errors need to be corrected if the accurate terms from the altimeter-calibration satellite link can be substituted into the altimeter-surface target link. Here is the process of the dual-link joint calibration.

B. Network Design and Optimization

A networking design and optimization phase were proposed to enhance the collaborative calibration capabilities of satellites.

Satellite networks employ multiple satellites with identical orbital inclinations and altitudes. Thus, the constellation is uniform and each satellite experiences similar perturbations, maintaining the configuration for a long time. Calibration satellite networking aims to calibrate multiple altimeter satellites spatially. Most altimeter satellites perform the observation tasks independently, such as the Jason series, whereas others form several satellite networks such as Sentinel-3A and Sentinel-3B. This means that most altimeter satellites do not have a collaborative relationship and their orbit distributions are not uniform.

Currently, there are no examples of in-orbit applications for calibration satellite networking. A good solution is to select one or several of the most effective orbits in the simulation as the core of the calibration satellite network. Subsequently, a few calibration satellites are launched for in-orbit testing, and the remaining calibration satellites are launched at designated positions to form a network. This reflects one of the benefits of satellite networks: Enhancing the overall flexibility and resilience of the systems. However, because of the small observable width of altimeter satellites and the influence of perturbations on their orbits, using a uniformly distributed satellite network considerably reduces the efficiency of the calibration satellite network.

The networking should be nonuniform to maximize the utilization of calibration satellites, suggesting a time-varying constellation configuration. Therefore, at the beginning of the constellation design, it is necessary to consider the specific altimeter satellites to be serviced and their lifespans in orbit before simulating the entire lifespan to determine the orbit parameters of the calibration satellites.

Traditional satellite networking methods are aimed at satellites that conduct Earth observation or serve ground targets, with coverage performance being a common design specification. Geometric analysis is often used to design satellite constellations by analyzing the relationship between satellite trajectories and ground coverage. The uniformly distributed inclined circular orbit plane design method proposed by Walker [31], [32], [33] is a classical method that has been widely used.

The drawback of traditional design methods is that the design approach is fixed, making it difficult to obtain optimal or near-optimal solutions. With the increasing complexity of space missions and the development of modern optimization algorithms, many studies have applied modern optimization algorithms to satellite constellation design. The purpose of establishing a calibration satellite network is to serve space targets.

TABLE I
PROCESS OF SATELLITE NETWORK DESIGN USING NSGA-II

1. Initialize Population(P)
2. Set mutation probability (p-mut)
3. Set maximum number of generations (G-max)
4. Input: Orbit elements of the satellite (O)
5. while (generation less than G-max) do
a. Propagate orbit elements (O')
b. Calculate fitness of P (F(P))
c. Selection, crossover, and mutation to generate offspring (P-offspring)
d. Calculate fitness of P-offspring (F(P-offspring))
e. Merge populations (Union of P and P-offspring)
f. Non-dominated sorting and calculate crowding distance (D)
g. Select elite individuals to form new parent population (P-new)
h. generation = generation + 1
i. if (termination condition met) then
j. Output: Results from P-new
k. Break loop
end if
6. end while

TABLE II
RANGE OF THE ELEMENTS

Elements	Range
Altitude	400-A km
Inclination	0-180°
RAAN	0-360°
True anomaly	0-360°

Therefore, when optimizing the network design, it is necessary to consider many factors such as the service frequency, number of serviceable satellites, and cost of the calibration satellites. This is essentially a multiobjective optimization problem under multiple constraints. In multiobjective optimization problems, there often exist multiple goals that conflict with each other, which means it is difficult to find a solution that simultaneously optimizes all objectives. Therefore, what we seek is a set of solutions that achieve a balance among the various objectives. This set is known as the Pareto solution set, or Pareto Front, which provides a collection of feasible solutions that represent different tradeoffs among the objectives, allowing decision-makers to choose the solution that best aligns with their preferences. An improved genetic algorithm is suitable for solving these problems. Therefore, this study uses the NSGA-II [22] to optimize the design of the calibration satellite network. The flowchart of the algorithm is illustrated in Table I.

1) *Initialization*: Initialization included initializing the population, setting the initial mutation probability, and maximizing the number of generations. For population initialization, it is necessary first to set the number of individuals, then randomly generate the orbit of the calibration satellites, and finally encode the orbit parameters. Encoding unifies multiple parameters into a data string to facilitate subsequent crossover and mutation operations. There are many methods of encoding. The objective of the constellation design is the optimization of the orbit elements of the calibration satellites, including the altitude, inclination, right ascension of the ascending node, and true anomaly. This study adopts a real-number encoding method, which has the advantage of obtaining high-precision orbit elements while facilitating subsequent orbit propagation and related calculations. For calibration, the altitudes of the calibration satellites should be lower than those of the satellites being calibrated. In addition, in practical engineering, if the satellite's altitude is too low, it will quickly reduce owing to atmospheric drag, resulting in a short satellite lifespan. Therefore, the minimum altitude of the calibration satellites is set at 400 km. If the minimum altitude among the satellites being calibrated is A km, the range of elements of the calibration satellites, considering the minimum altitude among the satellites as A km, is expressed in Table II.

2) *Propagating the Orbit Elements of the Satellite*: Before calculating fitness, the satellite orbit must be propagated. There are several methods for satellite orbit propagation, and while numerical integration methods can be employed, it is more advisable to use established commercial software for orbit propagation, such as STK (Satellite Tool Kit) and SPICE (Spacecraft Planet Instrument C-matrix Events). The satellite orbit propagation model only considers the perturbation caused by the J2 term of the Earth's gravitational field. This can speed up the algorithm and simulate the actual operation of satellites in orbit to a certain extent. It should be noted that when higher precision in orbit prediction is required, more perturbation factors must be considered. After all the calibration satellites in the network have completed orbit propagation, the number of satellites that can be calibrated and the total number of calibration times during the simulation period are calculated.

3) *Fitness*: Fitness is used to evaluate the superiority of individuals in a population. In this study, two fitness values are set: the total number of services provided and the number of satellites that can be serviced by the calibration satellite network. In both cases, the performance improves as the number increases.

4) *Nondominated Sorting, Crowding Degree*: Nondominated sorting is based on the dominant relationship between individuals fitness values in the population. First, we identify all nondominant individuals in the population in the first layer. These individuals represent the optimal solutions. The remaining individuals are then grouped into further layers using the above method. Finally, the crowding distance for each individual in each layer is calculated. The crowding distance represents the density of neighboring individuals in the current layer and can be used to compare two individuals in the same layer during the follow-up selection operation.

5) *Selection, Crossover, and Mutation*: The selection operation simulates the rule of survival of the fittest, such that individuals with better fitness have a higher probability of producing offspring. Of the many selection methods, tournament selection is adopted in this study. Two individuals are used for each comparison. Based on the results of the previous step, if the individuals are in different layers, the individual with a higher nondominated level is selected. If the individuals are in the same layer, the individual with a smaller crowding distance is selected. The selected population evolves toward the Pareto-optimal solution set. Then, the crossover is used to generate offspring, followed by the mutation operation. In this study, the crossover adopted is the partial match crossover. A random corresponding parameter in the parent is exchanged to produce the offspring. Moreover, random mutation method is used to randomly mutate the orbital elements of the individuals.

6) *Elite Strategy*: Elite strategy is used to ensure that the best individuals found so far are preserved in the population. This is done by directly copying the top performers from one generation to the next without undergoing crossover or mutation. The purpose of elite strategy is to prevent the algorithm from converging too quickly to local optima and to enhance its ability to explore the solution space globally. This study adopts an elite strategy to avoid the loss of superior individuals. The parent generation is mixed and offspring are generated to form a new population to expand the sample space. Then, we perform nondominated sorting and crowding degree calculations on the obtained new population. The supreme individuals are selected to form a new population according to the number of individuals in the initial population.

IV. ANALYSIS AND RESULTS

A. Accuracy Analysis

To verify the feasibility of the method based on calibration satellites, it is necessary to analyze the error terms of the expression of the backscatter coefficient, including the speed of light c , pulsewidth τ_p , π , distance from the altimeter to the calibration satellite R_s , and surface target R ; no further calibration is required. The atmospheric attenuation error depends on a model that is constantly updated.

However, many terms, such as the antenna pattern, echo digital output of the altimeter from the calibration satellite and surface target, and the backscatter coefficient of the calibration satellite can be corrected using the calibration satellite. It can be further corrected by increasing the number of calibration satellites, which is the primary consideration in the error analysis in this study.

Thus, the backscatter coefficient can be rewritten as follows:

$$\sigma_0 = K(\sigma) \frac{DN_A}{DN_{At}} \frac{1}{L_{pt}} f_{alt}^2(\theta_A, \phi) f_{trans}^2(\theta_A, \phi) \sigma_{trans} \quad (12)$$

where $K(\sigma)$ is the determinant in the backscatter coefficient that does not need to be corrected and is expressed as follows:

$$K(\sigma) = \frac{R^3}{R_s^4} \frac{1}{c\tau_c\pi}. \quad (13)$$

To obtain the results of the dB order, we take the logarithm of the backscatter coefficient in (12) and assume that any of the following are error sources (an example here is σ_{trans}):

$$10 \lg \sigma_0^* = 10 \lg W(\sigma) + 10 \lg \sigma_{trans} + \Delta\sigma_{trans} \quad (14)$$

where the remaining term in the backscatter coefficient $W(\sigma)$ is expressed as follows:

$$W(\sigma) = K(\sigma) \frac{DN_A}{DN_{At}} \frac{1}{L_{pt}} f_{alt}^2(\theta_A, \phi) f_{trans}^2(\theta_A, \phi). \quad (15)$$

The units of the backscatter coefficient are converted directly into the representation dB as follows:

$$\sigma_0 + \Delta\sigma_0 = W + 10 \lg \sigma_{trans} + \Delta\sigma_{trans}. \quad (16)$$

According to the ‘‘uncertainty principle,’’ no measurement can achieve absolute value, and the only way is to increase the times

TABLE III
DATA FROM SIMULATION EXPERIMENTS

Error Terms	value
Altimeter antenna pattern error	0.2 dB
Calibration satellite dish pattern error	0.1 dB
Calibration satellite backscatter coefficient error	0.15 dB
Surface target digital output	0.1 dB
Calibration satellite digital output	0.05 dB

TABLE IV
INITIAL ORBIT ELEMENTS OF THE FIVE ALTIMETER SATELLITES

Num	Altitude (km)	Inclination (°)	RAAN (°)	True Anomaly (°)
1	7343.85	99.34	50	40
2	7328.58	66	18	29
3	7328.58	80	18	219
4	7075.14	98.2	156	168
5	6992.14	97.9	44	154

of measurements and obtain the average value. The calibration method proposed in this article is based on the above principle: most calibration satellites are arranged in orbit lower than the altimeter; thus, under the coordination of the orbital networking design, each calibration satellite can serve the altimeter. With the increase in calibration satellites as shown in Fig. 5, the calibration accuracy will gradually improve. According to the weighted arithmetic mean geometric inequality, if n calibration satellites exist, the error term described above can be expressed as follows:

$$\Delta\sigma_0 \leq \frac{1}{2} 10 \lg \frac{\sigma_{trans}}{n}. \quad (17)$$

According to the analysis of an error source (plus and minus in the same way) and assuming that the entire system has m error terms with n calibration satellites, the error analysis expression for the entire system can be derived as follows:

$$\begin{aligned} \Delta\sigma_0 &= \sum_m \frac{1}{2} (10 \lg \Delta_m - 10 \lg n) \\ &\leq \frac{\sum_m |\max\{10 \lg \Delta_m\}|}{2} - \frac{m}{2} 10 \lg n. \end{aligned} \quad (18)$$

The error ranges used in altimeters are sorted, as shown in Table III for the Monte Carlo simulation for verification.

As shown in Fig. 6, the Monte Carlo simulation is executed for 100 iterations. The error results indicate that with the increase in the number of calibration satellites, the accuracy of the backscatter coefficient improves with increasing number of calibration satellites. The upper and lower bounds of the standard deviation are also given in the figure.

B. Network Simulation Results

First, a single calibration satellite is simulated to serve multiple satellites from January 1, 2024, to February 28, 2024, in coordinated universal time (UTC). Five altimeter satellites are set up with initial orbit elements, as shown in Table IV.

The initial number of individuals in the population is 30, the maximum number of generations is 200 generations, the offspring multiple is 0.5 times the parent population size, and

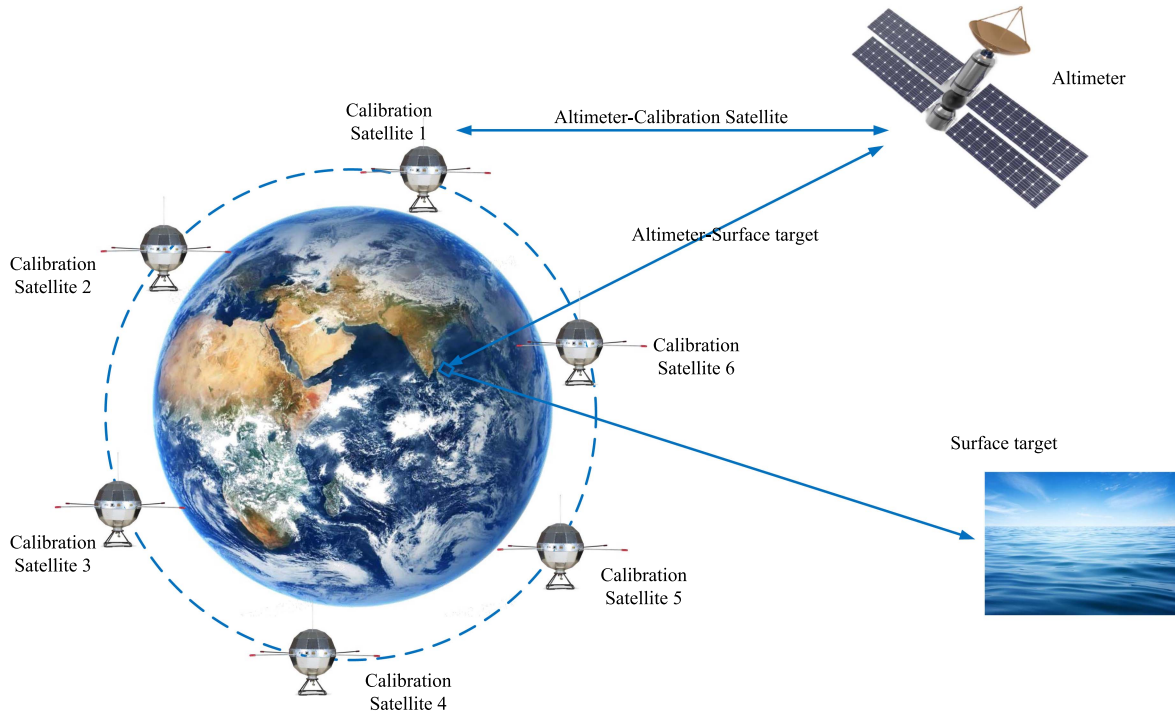


Fig. 5. Schematic of the multitransponder-assisted calibration system.

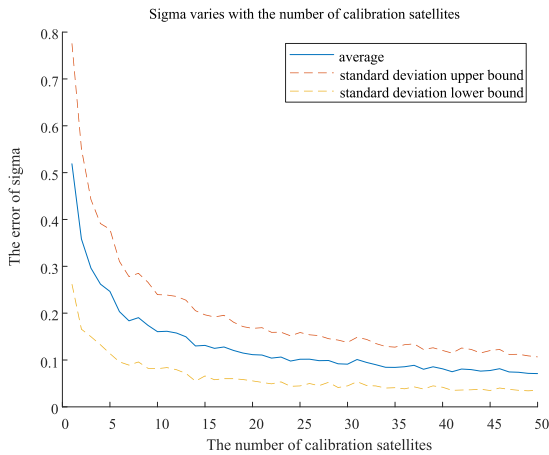


Fig. 6. Schematic of backscatter coefficient accuracy as a function of the number of calibration satellites.

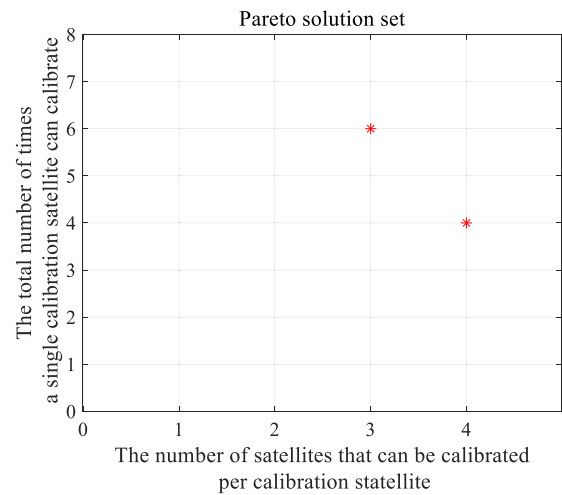


Fig. 7. Pareto solution set.

TABLE V
ORBIT ELEMENTS OF TWO CALIBRATION SATELLITES

Num	Altitude (km)	Inclination (°)	RAAN (°)	True Anomaly (°)
1	6822.43	82.49	13.77	157.78
2	6914.51	80.62	311.07	51.45

the mutation probability is 0.8. The obtained Pareto solution set is shown in Fig. 7.

The orbital elements of the calibration satellites are listed in Table V. The Pareto solution set shows that the total number of calibration times for a single calibration satellite can calibrate and the number of satellites that can be calibrated by each calibration satellite cannot be optimized simultaneously.

This, in multiobjective optimization problems, multiple sub-objectives cannot be optimized simultaneously. The two points on the graph represent two nondominated solutions, indicating that both are optimal solutions. However, each solution achieves its maximum value in different subobjectives.

In two months, a single calibration satellite can be used to calibrate up to four altimeter satellites with a maximum of four calibrations or up to three altimeter satellites with a maximum of six calibrations. When using multiple calibration satellites to calibrate a single altimeter satellite, the initial orbit elements of the altimeter satellite are given by Satellite 1 in Table III; the simulation time is from January 1, 2024, to January 31,

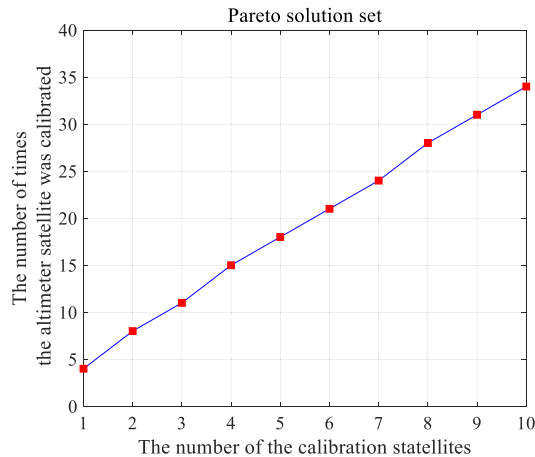


Fig. 8. The relationship between the number of times the altimeter satellite be calibrated and the number of calibration satellites.

TABLE VI
ORBIT ELEMENTS OF TEN CALIBRATION SATELLITES

Num	Altitude (km)	Inclination (°)	RAAN (°)	True Anomaly (°)
1	6841.59	80.63	264.96	6.90
2	6733.36	80.66	259.01	98.56
3	6824.41	69.22	279.45	70.12
4	6857.18	83.07	321.69	121.00
5	6729.80	82.54	239.15	246.04
6	6701.90	87.44	258.43	185.25
7	6722.49	79.65	254.12	142.25
8	6790.05	81.59	253.30	191.46
9	6678.29	85.50	271.90	304.73
10	6717.95	84.31	249.73	235.47

2024, UTC. The other simulation conditions are identical to those described above. The simulation results are presented in Fig. 8, and the orbit elements of the calibration satellites are shown in Table VI.

The simulation ranges from a single-satellite network to a two-satellite network and finally to a ten-satellite network. Because only one altimeter satellite was calibrated, the optimization goal was only to optimize the service frequency of the altimeter satellites. During the simulation period, a single calibration satellite could calibrate the altimetry satellite a maximum of four times, whereas ten calibration satellites could calibrate the altimetry satellite a maximum of 34 times. As the number of calibration satellites increases, the number of calibrated altimeter satellites also increases.

V. CONCLUSION

This study focuses on a novel altimeter calibration system based on calibration satellites. The aim is to expand the original altimeter-surface target calibration link to the altimeter-calibration satellite and altimeter-surface target dual-link calibration process by deploying calibration satellites slightly below the altimeter.

This method moves the transponder from the ground to the calibration satellite based on the active calibration method base of the transponder. The signal expressions of the altimeter from the transponder and from the surface target are combined, and the

atmospheric and systematic errors are separated indirectly. The proposed networking optimization model based on NSGA-II also shows that an increase in calibration satellites increases the number of altimeter satellites being calibrated.

The proposed error separation method dramatically reduces the influence of systematic errors on the calibration process and provides more reliable atmospheric error data by differentiating the total and systematic errors when the default error is additive. This is expected to provide more reference for atmospheric model modeling in the future. The ultimate goal of the final calibration is not to obtain a relatively accurate backscatter coefficient but to enhance the utilization rate of satellite data and promote the development of hydrology and other fields by obtaining accurate backscatter coefficients.

REFERENCES

- [1] M. Korobkin and E. DSa, "Significant wave height in the Gulf of Mexico: Validation of Jason-1 measurement against buoy data," in *Proc. 12th Conf. Integr. Observing Assimilation Syst. Atmosph., Oceans, Land Surf.*, New Orleans, USA, 2008, pp. 1–4.
- [2] T. Jin et al., "Analysis of vertical deflections determined from one cycle of simulated swot wide-swath altimeter data," *J. Geodesy*, vol. 96, no. 4, 2022, Art. no. 30.
- [3] L.-L. Fu and A. Cazenave, *Satellite Altimetry and Earth Sciences: A Handbook of Techniques and Applications*. Amsterdam, Netherlands: Elsevier, 2000.
- [4] B. D. Tapley, G. H. Born, and M. E. Parke, "The seasat altimeter data and its accuracy assessment," *J. Geophysical Res.: Oceans*, vol. 87, no. C5, pp. 3179–3188, 1982.
- [5] R. E. Cheney, B. C. Douglas, and L. Miller, "Evaluation of geosat altimeter data with application to tropical pacific sea level variability," *J. Geophysical Res.: Oceans*, vol. 94, no. C4, pp. 4737–4747, 1989.
- [6] S. Biancamaria et al., "Validation of Jason-3 tracking modes over french rivers," *Remote Sens. Environ.*, vol. 209, pp. 77–89, 2018.
- [7] P. Bonnefond et al., "Calibrating the SAR SSH of Sentinel-3A and Cryosat-2 over the corsica facilities," *Remote Sens.*, vol. 10, no. 1, 2018, Art. no. 92.
- [8] N. Chen, G. Han, J. Yang, and D. Chen, "Hurricane sandy storm surges observed by HY-2A satellite altimetry and tide gauges," *J. Geophysical Res.: Oceans*, vol. 119, no. 7, pp. 4542–4548, 2014.
- [9] M. Li, C. Zhao, Y. Zhao, Z. Wang, and L. Shi, "Polar sea ice monitoring using HY-2A scatterometer measurements," *Remote Sens.*, vol. 8, no. 8, 2016, Art. no. 688.
- [10] J. X.-Wei, L. M.-Sen, and Z. Youguang, "An overview of hy-2 satellite ground application system," *Eng. Sci.*, vol. 6, pp. 4–12, 2014.
- [11] C. Zhu, J. Guo, C. Hwang, J. Gao, J. Yuan, and X. Liu, "How HY-2A/GM altimeter performs in marine gravity derivation: Assessment in the south China sea," *Geophysical J. Int.*, vol. 219, no. 2, pp. 1056–1064, 2019.
- [12] B. Greco, A. Martini, N. Pierdicca, and P. Ciotti, "A novel approach for absolute backscatter calibration of spaceborne altimeters," in *IGARSS 2000 IEEE 2000 Int. Geosci. Remote Sens. Symp. Taking Pulse Planet: Role Remote Sens. Manag. Environ. Proc.*, IEEE, 2000, pp. 2191–2193.
- [13] Y. Zhang, J. Jiang, H. Zhang, and D. Zhang, "Spaceborne imaging altimeter for topographic mapping," in *Proc. IGARSS IEEE Int. Geosci. Remote Sens. Symp. Taking Pulse Planet: Role Remote Sens. Manag. Environ. Proc.*, IEEE, 2000, pp. 2349–2351.
- [14] P. Moore and C. Murphy, "Inter-calibration of multi-satellite altimetric missions," *Adv. Space Res.*, vol. 25, no. 5, pp. 1099–1102, 2000.
- [15] P. Moore and P. Sterlini, "Cross-calibration of topex/poseidon, ers-2 and geosat altimetry," *Adv. Space Res.*, vol. 30, no. 2, pp. 233–239, 2002.
- [16] M. Shimada, O. Isoguchi, T. Tadono, and K. Isono, "PALSAR radiometric and geometric calibration," *IEEE Trans. Geosci. Remote Sens.*, vol. 47, no. 12, pp. 3915–3932, Dec. 2009.
- [17] N. Pierdicca et al., "Transponder calibration of the ENVISAT RA-2 altimeter ku band sigma naught," *Adv. Space Res.*, vol. 51, no. 8, pp. 1478–1491, 2013.
- [18] M. Roca, H. Jackson, and C. Celani, "RA-2 sigma-0 absolute calibration," in *Proc. ENVISAT Validation Workshop*, Frascati, Italy, H. Lacoste, Ed., 2003, pp. 1–15.

- [19] G. Brown, "The average impulse response of a rough surface and its applications," *IEEE Trans. Antennas Propag.*, vol. 25, no. 1, pp. 67–74, Jan. 1977.
- [20] G. Caudal, E. Dinnat, and J. Boutin, "Absolute calibration of radar altimeters: Consistency with electromagnetic modeling," *J. Atmos. Ocean. Technol.*, vol. 22, no. 6, pp. 771–781, 2005.
- [21] P. Pesece, H. Sünkel, and N. Windholz, "The use of transponders in altimetry," in *Proc. Gravity Geoid: Joint Symp. Int. Gravity Commission Int. Geoid Commission*. Springer, 1995, pp. 394–400.
- [22] K. Deb, A. Pratap, S. Agarwal, and T. Meyarivan, "A fast and elitist multi-objective genetic algorithm: NSGA-II," *IEEE Trans. Evol. Computation*, vol. 6, no. 2, pp. 182–197, Apr. 2002.
- [23] D. A. Shnidman, "Radar detection probabilities and their calculation," *IEEE Trans. Aerosp. Electron. Syst.*, vol. 31, no. 3, pp. 928–950, Jul. 1995.
- [24] Y. Bock et al., "Detection of crustal deformation from the landers earthquake sequence using continuous geodetic measurements," *Nature*, vol. 361, no. 6410, pp. 337–340, 1993.
- [25] H. Wheeler, "Small antennas," *IEEE Trans. Antennas Propag.*, vol. 23, no. 4, pp. 462–469, Jul. 1975.
- [26] P. F. MacDoran and G. H. Born, "Time, frequency and space geodesy: Impact on the study of climate and global change," *Proc. IEEE*, vol. 79, no. 7, pp. 1063–1069, Jul. 1991.
- [27] X. Jiang et al., "The HY-2 satellite and its preliminary assessment," *Int. J. Digit. Earth*, vol. 5, no. 3, pp. 266–281, 2012.
- [28] G. Wei, G. X.-Yan, X. X.-Yu, H.-G. Liu, X. C.-Dong, and D. Y.-Heng, "A transponder system dedicating for the on-orbit calibration of China's new-generation satellite altimeter and scatterometer," in *Proc. IEEE CIE Int. Conf. Radar*. IEEE, 2011, pp. 22–25.
- [29] X.-Y. Xu, W. Guo, H.-G. Liu, L.-W. Shi, W.-M. Lin, and Y.-H. Du, "Design of the interface of a calibration transponder and an altimeter/scatterometer," in *Proc. IEEE Int. Geosci. Remote Sens. Symp.*. IEEE, 2011, pp. 953–956.
- [30] K. Xu, J. Jiang, and H. Liu, "Hy-2a radar altimeter design and in flight preliminary results," in *Proc. IEEE Int. Geosci. Remote Sens. Symp.*. IEEE, 2013, pp. 1680–1683.
- [31] J. Walker, "Some circular orbit patterns providing continuous whole earth coverage," *J. Brit. Interplanetary Soc.*, vol. 24, pp. 369–384, 1971.
- [32] J. G. Walker, "Continuous whole-earth coverage by circular-orbit satellite patterns," *NASA Sti/recon*, Tech. Rep., 1977, vol. 78, p. 11169.
- [33] J. G. Walker, "Satellite patterns for continuous multiple whole-earth coverage," 1978. [Online]. Available: <https://api.semanticscholar.org/CorpusID:129591707>



Chenghao Lu (Graduate Student Member, IEEE) received the B.S degree in communication engineering from Hohai University, Nanjing, China, in 2022. He is currently working toward the Ph.D. degree in information and communication engineering with the School of Resources and Environment, University of Electronic Science and Technology, Chengdu, China. His current research interests include altimeter calibration system, vegetation parameter inversion using synthetic aperture radar (SAR) data, and interferometric SAR (InSAR) techniques.



Taoli Yang (Senior Member, IEEE) received the Ph.D. degree in signal processing from the National Key Laboratory of Radar Signal Processing, Xidian University, Xi'an, China, in 2014.

From January 2015 to February 2016, she was a Postdoctoral Research Fellow with the School of Electrical and Electronic Engineering, Nanyang Technological University, Singapore. She is currently an Associated Professor with the School of Resources and Environment, University of Electronic Science and Technology, Chengdu, China. Her current research interests include SAR/ISAR imaging, interferometric SAR, GRACE, and ground moving target indication.



Boxiang Zhang (Member, IEEE) received the M.Sc. degree from Harbin Institute of Technology, Harbin, China, in 2020.

He is currently an Engineer with the Millimeter Wave Imaging Technology Laboratory, Shanghai Institute of Satellite Engineering, Shanghai, China. His primary research interests focus on satellite orbit design, where he has been contributing to the development of innovative methodologies and applications in the field.



Hanwen Yu (Senior Member, IEEE) received the B.S. and Ph.D. degrees in electronic engineering from Xidian University, Xi'an, China, in 2007 and 2012, respectively.

He was a Postdoctoral Research Fellow with the Department of Civil and Environmental Engineering, National Center for Airborne Laser Mapping, University of Houston, Houston, TX, USA. He is currently a Full Professor with the School of Resources and Environment, University of Electronic Science and Technology of China, Chengdu, China, and an Adjunct Full Professor with the Academy of Advanced Interdisciplinary Research, Xidian University, and the Department of Engineering, University of Naples, Naples, Italy. He has authored more than 70 scientific articles and given scientific presentation about "Advanced Techniques in InSAR Phase Unwrapping" invited by the IEEE Geoscience and Remote Sensing Society (GRSS) Webinar in 2021. He reviewed more than 300 manuscripts for more than 20 different journals. His research interest focuses on InSAR, and this work has led to new insights into the worldwide deformation monitoring and topographic mapping.

Dr. Yu has been involved in IEEE (in general) and IEEE GRSS in particular. He was elected as a Best Reviewer of IEEE TRANSACTIONS ON GEOSCIENCE AND REMOTE SENSING in 2019. He was a recipient of several awards and honors from IEEE GRSS, including the 2022 Transactions Prize Paper Award, the Technical Program Committee Member, and the Session Chair of 2022 IGARSS, and the Principal Investigator of two IEEE GRSS 50.